Electronic Supplementary Information [ESI]

Multimodal breakup of double emulsion droplet under electric field

Muhammad Salman Abbasi[1], Ryungeun Song[1], Hyoungsoo Kim[2,*], and Jinkee Lee[1,*]

[1]School of Mechanical Engineering, Sungkyunkwan University, Suwon, Gyeonggi-do 16419, Republic of Korea

[2]Department of Mechanical Engineering, Korea Advanced Institute of Science and Technology (KAIST), Daejeon 34141, Republic of Korea

*Corresponding authors:

Professor Jinkee Lee Tel: +82-31-299-4845, E-mail address: lee.jinkee@skku.edu

Professor Hyoungsoo Kim Tel: +82-42-350-3049, E-mail address: hshk@kaist.ac.kr

The supplementary information provides details about the validation results for experimental setup, droplet fabrication method, simulation technique, the dynamics of silicone oil-castor oil-silicone oil (SO-CO-SO) double emulsion, core droplet migration inside the shell, calculation of electric and hydrodynamic stresses at the core side apex, lubrication model for film drainage and unstable bimodal breakups. It also includes six supplementary videos.

I. Validation of experimental setup

The validation of the current experimental setup is shown in **Fig. S1** in which a drop of silicone oil suspended in castor oil without any dopant is subjected to electric field. The measured deformation is then compared with the Taylor theory[1] and results from other studies.[2, 3]

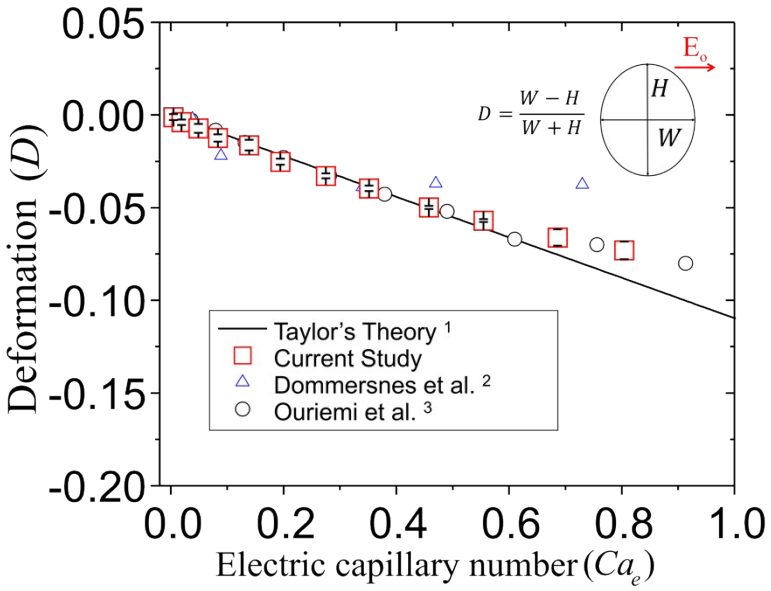

Fig. S1 Comparison between Taylor's theory and experimental setup by comparing the results of deformation obtained for emulsion droplet of silicone oil with no core (single emulsion droplet), i.e., $\beta = 0$ suspended in castor oil under electric field. The radius of the droplet is 1 mm.

II. Droplet fabrication process

The detailed process of droplet fabrication used in experiments and the fabricated double emulsion droplets are illustrated in **Fig. S2**.

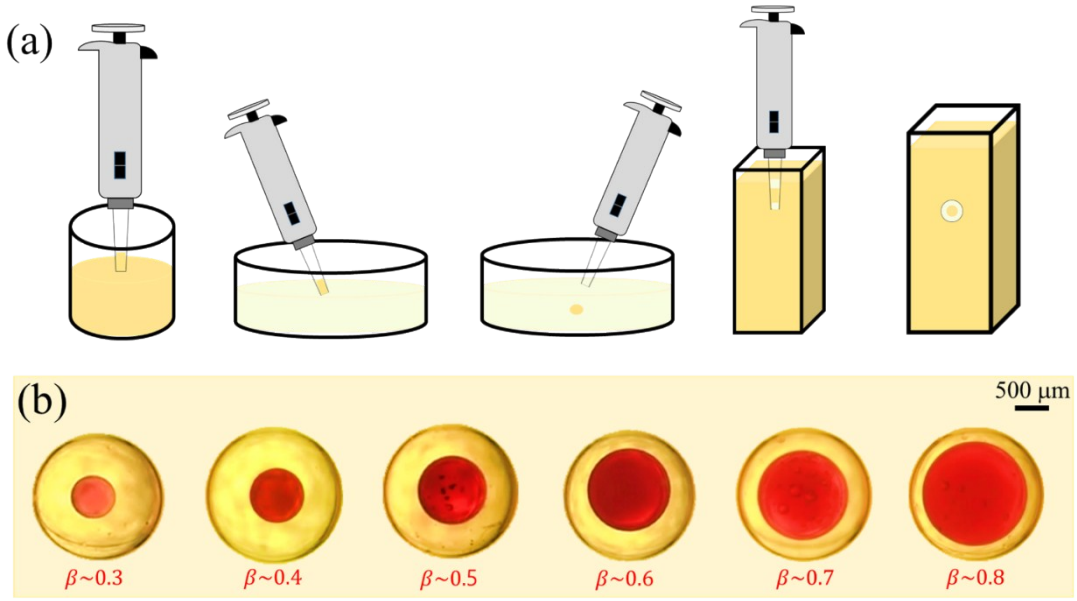

Fig. S2 (a) Sketch of fabrication process of double emulsion droplets (b) Different β for various double emulsion droplets by varying the volume fraction of the core. β is the ratio of the core radius to the shell droplet radius.

III. Simulation method and governing equations

Here, we present the details of the simulation method and governing equations used for studying the dynamics of double emulsion droplets under electric field. The numerical domain is shown in **Fig. S3.**

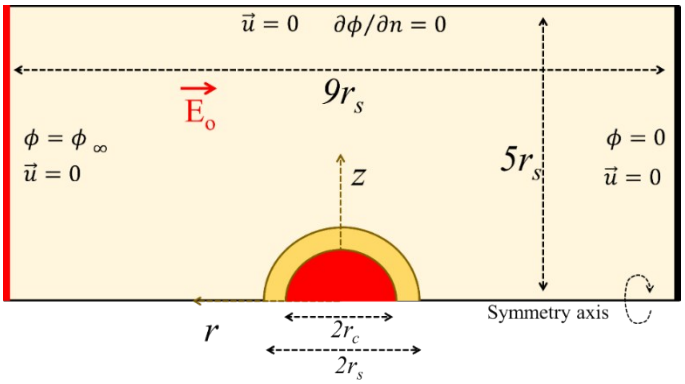

Fig. S3 Computational domain for the model problem used for the numerical simulation with boundary conditions.

Governing equations

a) Level set method

Here, we use the conservative level set method for tracking the core-shell and shell-ambient interfaces. The interface between any of the two liquids is evolved by a fixed contour of a level set function $\xi = 0.5$ in the level set equation, given as

$$\frac{\partial \xi}{\partial t} + \nabla \cdot (\vec{u}\,\xi) = \varpi \nabla \cdot \left(\Lambda \nabla \xi - \xi(1-\xi)\frac{\nabla \xi}{|\nabla \xi|} \right). \quad \text{(S1)}$$

where $\vec{u}$ is the velocity field inside the domain, Λ is the parameter that controls the thickness of the interface, ϖ is the stability parameter known as re-initialization parameter, and $\xi(1-\xi)\frac{\nabla\xi}{|\nabla\xi|}$ is known as the artificial flux. The term in the Laplacian in equation (S1) is a diffusion term. This is countered by the divergence of flux.

In this problem, density(ρ), viscosity(μ), conductivity (σ), and permittivity (ε) are expressed by the function of the level set variable ξ represented as

$$\rho = \xi(\rho_s - \rho_c) + \rho_c, \qquad \rho = \xi(\rho_s - \rho_a) + \rho_a \tag{S2a}$$

$$\mu = \xi(\mu_s - \mu_c) + \mu_c, \qquad \mu = \xi(\mu_s - \mu_a) + \mu_a \tag{S2b}$$

$$\sigma = \xi(\sigma_s - \sigma_c) + \sigma_c, \quad \sigma = \xi(\sigma_s - \sigma_a) + \sigma_a \tag{S2c}$$

$$\varepsilon = \xi(\varepsilon_s - \varepsilon_c) + \varepsilon_c, \quad \varepsilon = \xi(\varepsilon_s - \varepsilon_a) + \varepsilon_a \tag{S2d}$$

where subscripts *c, s*, and *a* denote the core, shell, and ambient liquids, respectively. The level set function is "0" for the core and ambient liquids and changes to "1" for the shell liquid.

b) Momentum equations

To study the dynamics of double emulsion droplets under a direct current electric field we couple the incompressible Navier-Stokes equations with the Level set equation, combined with the governing equation of the electric field and electric stresses. For incompressible flow, the continuity equation and the Navier-Stokes equations are given as

$$\nabla.\vec{u} = 0, \tag{S3a}$$

$$\rho\left(\frac{\partial\vec{u}}{\partial t} + (\vec{u}\cdot\nabla)\vec{u}\right) = \nabla\{-pI + \mu[(\nabla\vec{u}) + (\nabla\vec{u})^T]\} + \vec{F}_{st} + \vec{F}_e, \tag{S3b}$$

where F_e is the volumetric force due to Maxwell stress tensor whereas F_{st} is the surface tension force.

c) Leaky dielectric model

When all of the liquids involved are leaky dielectrics under the quasi-electrostatics assumption, the conservation of free charges can be written as

$$\frac{\partial q_f}{\partial t} + \nabla.\vec{J} = 0, \tag{S4}$$

where we assume that all the liquids follow the Ohmic conduction law, and the current density $\vec{J}$ is related with electric field $\vec{E}$ by $\vec{J} = \sigma\vec{E}$ where σ is the electrical conductivity as defined by equation (S2c). By Gauss's law, we can obtain the following equation

$$\nabla \cdot \left(\varepsilon_o \varepsilon \frac{\partial \vec{E}}{\partial t} + \sigma \vec{E} \right) = 0 \quad \text{(S5)}$$

Electric field $\vec{E}$ is governed by

$$\vec{E} = \nabla \phi, \quad \text{(S6)}$$

where ϕ is electric potential. The electric force $F_e = \nabla \cdot \sigma_M$ can be calculated by taking the divergence of Maxwell stress tensor $\sigma_M = \varepsilon(\vec{E}\vec{E} - E^2 I/2)$. Since ε is the function of the level set function whose value changes across the interface by equation (S2d), the electric force due to Maxwell stresses only acts at the liquid-liquid interface.

IV. Dynamics of silicone oil-castor oil-silicone oil (SO-CO-SO)

We consider that the shell is more conducting than the ambient liquid $R_{23} >> 1$ and $R_{12} << 1$ due to $R_{12} = 1/R_{23}$. **Fig. S4** shows the electric potential lines, flow patterns, surface charge distribution, and Maxwell stress force. Here, the electric potential (ϕ) does not penetrate through the shell/ambient interface and are more concentrated in the ambient liquid; thus, it is unable to reach the core/shell interface effectively. This causes the magnitude of liquid flow and the corresponding core/shell deformation to be very small due to weak electrical Maxwell stress, which depends on the electrical potential.

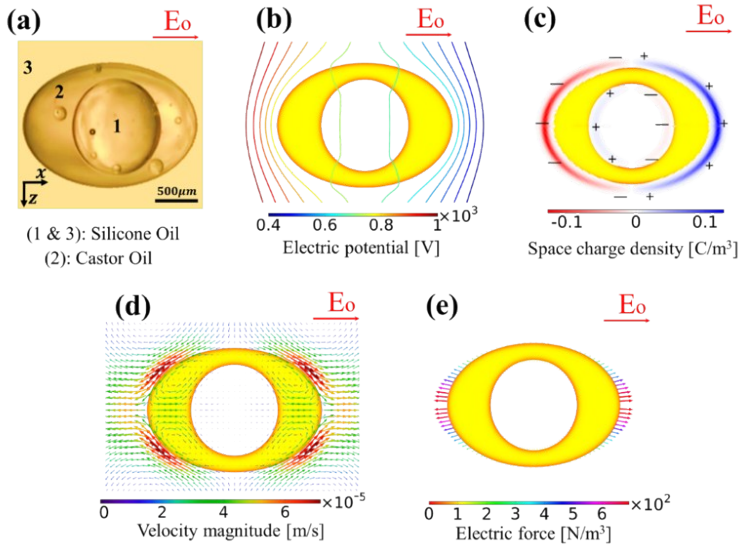

Fig. S4 Deformation of silicone oil–castor oil-silicone oil (SO-CO-SO) double droplet. (a) Experimental result. (b-e) Numerical results: (b) Electric potential contours, (c) Space charge density, (d) Flow patterns and velocity vectors, and (e) Electric force vectors due to Maxwell stresses. For the detailed experimental and numerical conditions;

$Ca_{23} = 0.2345, \beta = 0.65, S_{23} = {}^{1}/_{S_{12}} = 1.47, R_{23} = {}^{1}/_{R_{12}} = 34.48, and\ \Gamma_{23} = {}^{1}/_{\Gamma_{12}} = 0.80.$

The electrohydrodynamic behavior of silicone oil–castor oil-silicone oil (SO-CO-SO) under strong electric fields is shown in **Fig. S5**. The core does not deform. The outer shell elongates and eventually breaks up. When the electric fields are further increased, the penetration depth of the electric potential becomes weaker and it makes the core/shell interfaces to be not sensitive. However, large accumulation of charges and concentration of electrical potential at the shell/ambient cause it to deform in a prolate manner and eventually shell/ambient interface starts streaming. Here, the breakup occurs without interfacial coalescence.

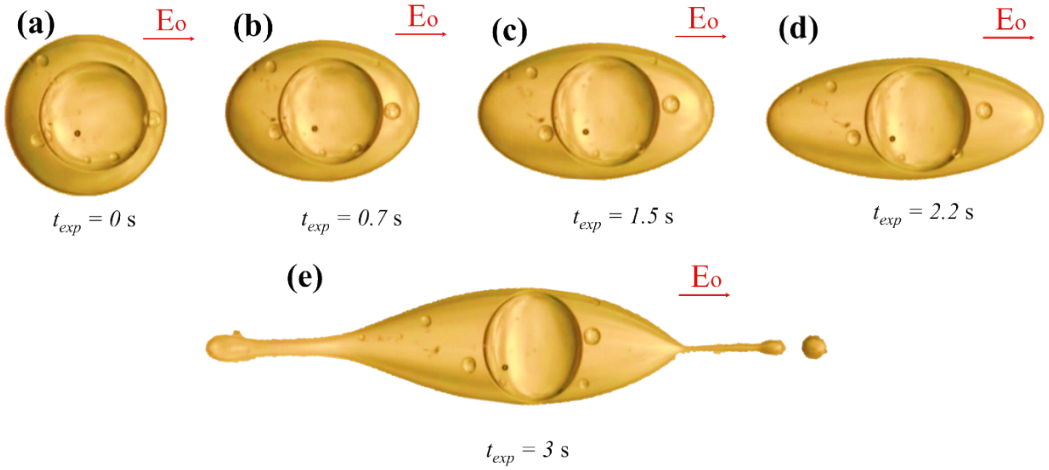

Fig. S5 Breakup of the outer shell while the core seems undeformed. The experimental conditions are $Ca_{23} = 0.2968, \beta = 0.65, S_{23} = {}^{1}/_{S_{12}} = 1.47, R_{23} = {}^{1}/_{R_{12}} = 0.029, and\ \Gamma_{23} = {}^{1}/_{\Gamma_{12}} = 0.80.$

V. Core droplet migration inside the shell

To check the effect of the droplet eccentricity and the dielectrophoretic force on the motion of the core droplet inside the shell liquid, we performed additional experiments. For this case, we considered a droplet of castor oil dispensed in an unbounded silicone oil under a direct current electric field. The results are as shown in Fig. S6.

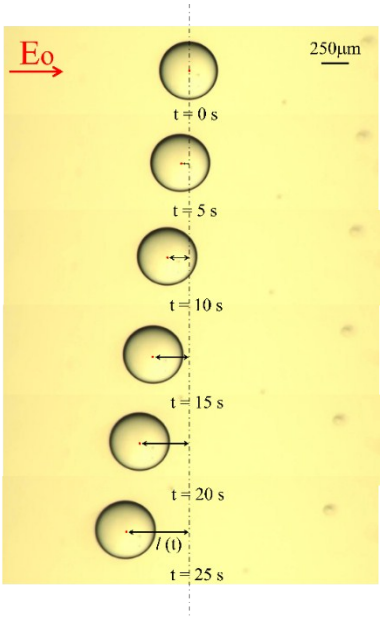

Fig. S6 Electro-migration of castor oil droplet dispensed in unbounded silicone oil under uniform direct current electric field ($E_o = 0.95$ kV/cm). l (t) is the distance travelled from the initial position where the red dot indicates the centroid position of the droplet in each frame.

We observed that the droplet slightly deforms and it moves linearly with respect to the electric field strength. Since the electric field is uniform, dielectrophoretic effects are negligible. Therefore, this motion of the droplet should be due to the electrophoretic effects that warrants the existence of an inevitable net charge. Such a slow electro-migration was also revealed for a single phase droplet under uniform electric field by the primary studies on the topic, which was not explained by the previous research results based on theoretical analysis.[1, 4]

Additionally, we performed numerical simulations for an eccentric castor oil core without any net charge in silicone oil shell suspended in castor oil, and the numerical results are as shown in Fig. S7.

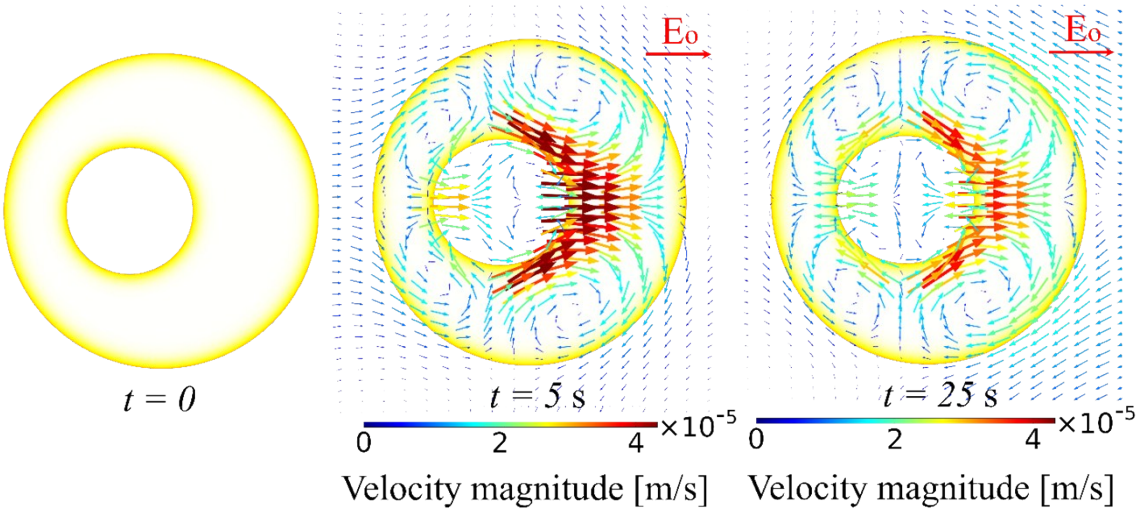

Fig. S7 Eccentric castor droplet in silicone shell under electric field

It can be seen that the core very slightly moves towards the centroid position.

We believe that the electro-migration of core inside the shell is due to some charge at the core interface. Such a charge may arise due to the following possible reasons.

1) From the ion adsorption[5, 6]

Taylor's leaky dielectric model (TLDM)[1] treats electrical current based on static ohmic conduction without considering the underlying ionic dynamics and the charge convection effects that leads to electric monopolar charge layer (EML) at the interface. A more thorough description of electrohydrodynamic phenomena in low conducting media should thus be based on the Nernst-Planck (NP) equations of ionic transport where electrical double layers (EDLs) at the material interfaces play a key role. Thus, the classical TLDM should be coupled with NP equations. Otherwise, the prediction will be poor.[5, 6]

2) Droplet dispensation using conventional pipetting[7]

In experimental studies, droplets of micro-liter volume are normally dispensed by using micro-pipettes. Recently, it has been reported that the droplets dispensed by using conventional pipetting are charged. This charge can occur due to the two possible mechanisms: a) Static charge can accumulate on the pipette tip due to friction associated with the liquid transports. b) Electrification of the inside surface of pipette tips due to ionization of surface groups. An electric double layer (EDL) with a negative charge will be created to conserve the electrical neutrality, if a positive surface charge develops on the pipette tip surface due to these mechanisms. Then, when the droplet is dispensed, the negative charge in the EDL can be carried away with the liquid and the positive charge can remain on the pipette tip surface.

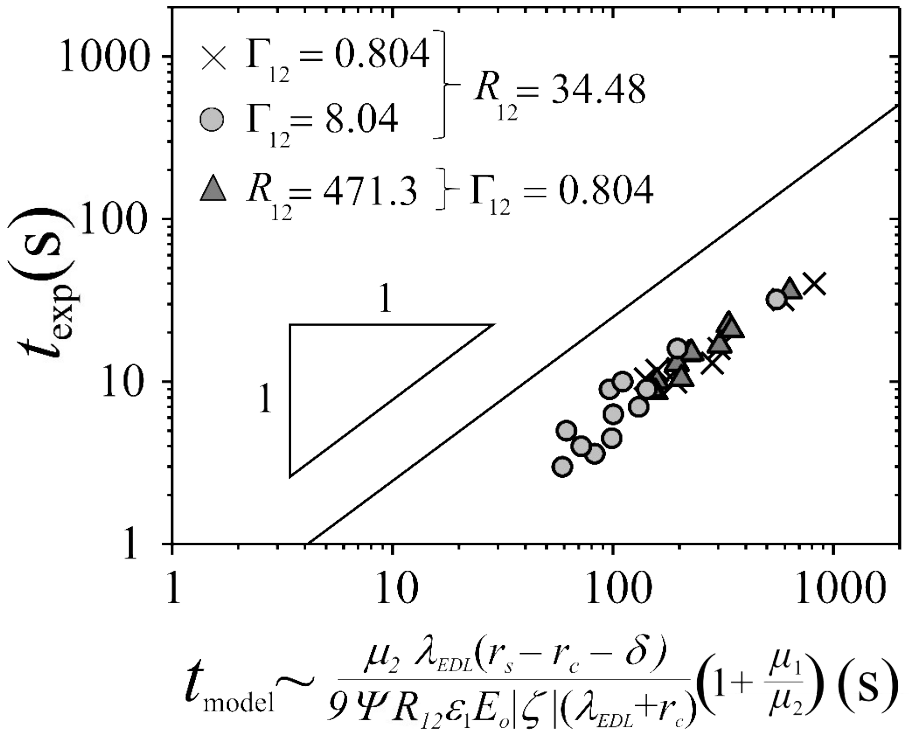

Fig. S8 Comparison of the drainage time scale between theory and experimental results for the core droplet approaching the shell interface at the unidirectional breakup mode.

We investigate the breakup time scale as a function of core droplet position by considering $\delta/(r_s - r_c) \neq 0$, where δ is the offset of the core droplet from the center position of the shell droplet (see Fig. S8). For this case, we estimate the total time duration for the migration of the core droplet by considering the balance between the drag force (F_d) and electrophoretic force (F_e) under a uniform electric field. For the immersed core droplet in the shell fluid, the drag force can be scaled as $F_D \sim 4\pi r_c \mu_2 U(1 + \Gamma_{12})$ where U is the terminal velocity and $\Gamma_{12} = \mu_1/\mu_2$. The terminal velocity U is scaled as $\sim (r_s - r_c - \delta)/t_{model}$, where t_{model} is the total time duration for the migration and $r_s - r_c - \delta$ is the total migration distance before the rupture. In the manuscript, ℓ is $(r_s - r_c - \delta)$. Alternatively, the electrophoretic force (F_e) acting on the spherical core is given as $F_e = QE_{r=r_c}$, where Q is the net charge on the core per volume and $E_{r=r_c}$ is the electric field acting at the core interface.[8] From the solution of the governing Laplace equation ($\nabla^2 \phi_j = 0$) of charge conservation with specific boundary conditions, where the index j indicates the shell liquid, $E_{r=r_c} = 9\Psi R_{12} E_o$ at the side apex of the core, where $\Psi = 1/[(R_{12} + 2)(R_{23} + 2) + 2\beta^3(R_{12} - 1)(R_{23} - 1)]$ and E_o is the externally applied electric field gradient along the droplet. Here, we do not account for space charges in the calculation of the electric field and we assume the electric field to be constant over the entire core surface. Here, we assume that the net charge value is approximated as $Q \sim 4\pi r_c^2 \varepsilon_1 |\zeta| (1/r_c + 1/\lambda_{EDL})$, where ζ is the zeta potential and λ_{EDL} is the thickness of electrical double layers. Debye length for the considered system can be calculated from the relation[9] ($\lambda_{EDL} = \sqrt{\frac{\varepsilon K_b T}{e^2 z^2 n}} = \sqrt{\frac{D \times \varepsilon}{\sigma}}$), where $D = \mathrm{M} K_b T/ez$ is the ion diffusivity and $\sigma = \mathrm{M} nez$ is the electric conductivity. Here, M is the ion mobility ($= v_d/E_o$; v_d is the drift velocity and E_o is the applied electric field), K_b is the Boltzmann constant ($1.38 \times 10^{-23} J/K$), e is the electric charge ($1.602 \times 10^{-19} C$) and z is the valence of ions. If we consider the sodium ion at 298 K with $E_o \sim 1$ kV/m, the diffusivity in castor oil comes to be ~10^{-12} m^2/s, and with the values for permittivity and conductivity, the Debye length can be estimated as 1.8 μm. The zeta potential is *O* (1 mV) [10-12] for a liquid-liquid interface. Therefore, the total migration time scale of the core droplet is

$$t_{model} \sim \frac{\mu_2 \lambda_{EDL} (r_s - r_c - \delta)}{9\Psi R_{12} \varepsilon_1 E_o |\zeta| (\lambda_{EDL} + r_c)} \left(1 + \frac{\mu_1}{\mu_2}\right). \tag{S7}$$

Then, we compare the theoretical and experimental results in Fig. S8. The theoretical model [equation (S7)] shows the same power-law trend and can reasonably predict the order of magnitude of migration timescale.

VI. Calculation of Maxwell stress and hydrodynamic stress jumps at the side apex of the core

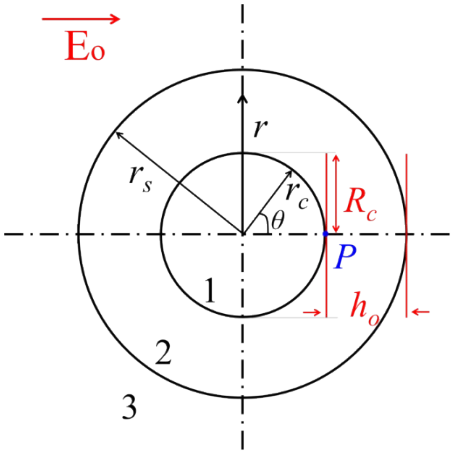

Fig. S9 Schematic of a double emulsion droplet under direct current electric field. Notation and parameters are defined for the calculation of stresses at the side apex used in film drainage model.

We consider a side apex point (*P*) on the core of a double emulsion droplet as shown in the **Fig. S8** and calculate the electric Maxwell and hydrodynamic stress jumps

a) Maxwell stress calculation

The Maxwell stress jumps acting at the interface are the drivers behind the liquid flow circulations and the interface deformation. These stress jumps are evaluated from the Maxwell stress tensor given as

$$\sigma_M = \varepsilon\vec{E}\vec{E} - \varepsilon\vec{E}\cdot\vec{E}I/2. \tag{S8}$$

The stress jumps at the interface can be decomposed into tangential and normal components. The normal component of stress jump $\left\|\left(\sigma_M\cdot\vec{n}\right)\cdot\vec{n}\right\| = \left\|\varepsilon(\vec{E}\cdot\vec{n})^2 - \varepsilon(\vec{E}\cdot\vec{t})^2\right\|/2$ can further be simplified for core/shell interface as $\left\|\left(\sigma_M\cdot\vec{n}\right)\cdot\vec{n}\right\|_{12} = -\frac{1}{2}\varepsilon_o\left(\varepsilon_2{E_{n2}}^2 - \varepsilon_1{E_{n1}}^2\right) + \varepsilon_o\left(\varepsilon_2{E_{t2}}^2 - \varepsilon_1{E_{t1}}^2\right)$ where $E_t = -\partial\phi/\partial t$ and $E_n = -\partial\phi/\partial n$. Note that here $n \equiv r$ and $t \equiv \theta$, respectively. By the continuity of the normal component of the electric current density condition, $\sigma_1\partial\phi_1/\partial r = \sigma_2\partial\phi_2/\partial r$ and by the continuity of tangential component of electric stress at the interface, $E_{t1} = E_{t2}$, the stress jump can be described as

$$\left\|\left(\sigma_M\cdot\vec{n}\right)\cdot\vec{n}\right\|_{12} = -\frac{1}{2}\varepsilon_o\varepsilon_2\left(1 - \frac{S_{12}}{R_{12}^2}\right){E_{n2}}^2 - \varepsilon_o\varepsilon_2(S_{12} - 1){E_{t2}}^2. \tag{S9}$$

If we consider only at side apex ($\theta = 0$) and $E_{t2} = -\partial\phi/\partial r = 0$,

$$\left\|\left(\sigma_M\cdot\vec{n}\right)\cdot\vec{n}\right\|_{12} = -\frac{1}{2}\varepsilon_o\varepsilon_2\left(1 - \frac{S_{12}}{R_{12}^2}\right){E_{n2}}^2. \tag{S10}$$

The electric field components are obtained by the electric potential(ϕ) field in spherical coordinates such as

$$\vec{E}_i = -\left(\hat{r}\frac{\partial}{\partial r} + \hat{\theta}\frac{\partial}{r\partial\theta}\right)\phi_i \quad , \tag{S11}$$

where *i* =1, 2 and 3 for core, shell, and ambient liquid, respectively.

The electric potential (ϕ_i) for each phase is obtained by the solution of Laplace equation ($\nabla^2\phi_i = 0$) of the charge conservation with following boundary conditions: (1) $\phi_1(r_c,\theta) = \phi_2(r_c,\theta)$; (2) $\phi_2(r_s,\theta) = \phi_3(r_s,\theta)$; (3) $\sigma_1\partial\phi_1/\partial r(r_c,\theta) = \sigma_2\partial\phi_2/\partial r(r_c,\theta)$; (4) $\sigma_2\partial\phi_2/\partial r(r_s,\theta) = \sigma_3\partial\phi_3/\partial r(r_s,\theta)$; (5) $\phi_1(0,\theta)$ is bounded; (6) $\phi_3(r,\theta) = E_o r\cos\theta \quad where\ r\to\infty$. As a result, ϕ_1 and ϕ_2 are given as

$$\phi_1 = 9\Psi r E_o \cos\theta, \tag{S12a}$$

$$\phi_2 = 3\Psi(R_{12}+2)\left[\left(r/r_s\right) - \varsigma(r_s/r)^2\right] r_s E_o \cos\theta, \tag{S12b}$$

where $\Psi = 1/(R_{12}+2)(R_{23}+2) + 2\beta^3(R_{12}-1)(R_{23}-1)$, $\zeta = \beta^3(R_{12}-1)/(R_{12}+2)$.

Substituting equation (S11) into equation (S10) and subsequently combining with equation (S9) yields the normal electric stress component at the side apex *P*, such as

$$\frac{\partial}{\partial z}\left((\sigma_M\cdot\vec{n})\cdot\vec{n}\right) \simeq \left\|(\sigma_M\cdot\vec{n})\cdot\vec{n}\right\|_{12} = 81\Psi^2 S_{23}\left(S_{12} - {R_{12}}^2\right)\varepsilon_3 {E_o}^2/2 \quad . \tag{S13}$$

b) Hydrodynamic stress calculation

The hydrodynamic stress jump at the core side apex *P* stretching with velocity dh/dt could be given as

$$\frac{\partial}{\partial z}\left((\sigma_H\cdot\vec{n})\cdot\vec{n}\right) \simeq \left\|(\sigma_H\cdot\vec{n})\cdot\vec{n}\right\|_{12} = -\frac{2\mu_2\chi dh}{r\Gamma_{23}\,dt} \quad . \tag{S14}$$

where χ is a non-dimensional factor that incorporates effects of the volume fraction of the core to the shell and viscosity ratios of all phases. Here, we have calculated the value of χ by [13]

$$\chi = \frac{(2\beta^5 A - 6\beta^2 B - 8C - \beta^7 D)\Gamma_{23} - 3\beta^5 E\Gamma_{13}}{\beta^5 F} \quad , \tag{S15}$$

where A, B, C, D, E and F are the coefficients and can be calculated by the procedure as given from Table S1. [13]

Table S1. Calculated values of χ at different hydrodynamic conditions

β	Γ_{12}	Γ_{23}	χ
0.5	8.04	0.124	6.28
0.5	0.804	1.24	30.23

0.5	0.268	3.73	77.72

Total pressure at the apex could be the sum of electric and hydrodynamic stresses and is given as

$$p(0,t) \simeq \frac{81}{2}\Psi^2 S_{23}\left(S_{12} - {R_{12}}^2\right)\varepsilon_3 {E_o}^2 - \frac{2\mu_2 \chi dh}{r\Gamma_{23}\, dt}. \qquad \text{(S16)}$$

VII. Lubrication model for the thin film drainage in the double emulsion droplet

We analytically investigate the shell film thinning at the side before the rupture. In this case, we assume that the core droplet shape does not significantly change, and we ignore the hydrodynamic effects of the core liquid and the effects of space charge. We mainly focus on the thin film drainage at the thinnest part, which is the side apex where the Maxwell stresses are most significant due to the high electrical potential field. Based on the experimental observations, we used the lubrication model in which the gap is considered a thin film, and we assumed the flow in the film to be axisymmetric. This film drainage method applied to the deformable droplet case is the so-called Stefan-Reynolds parallel film model. [14]

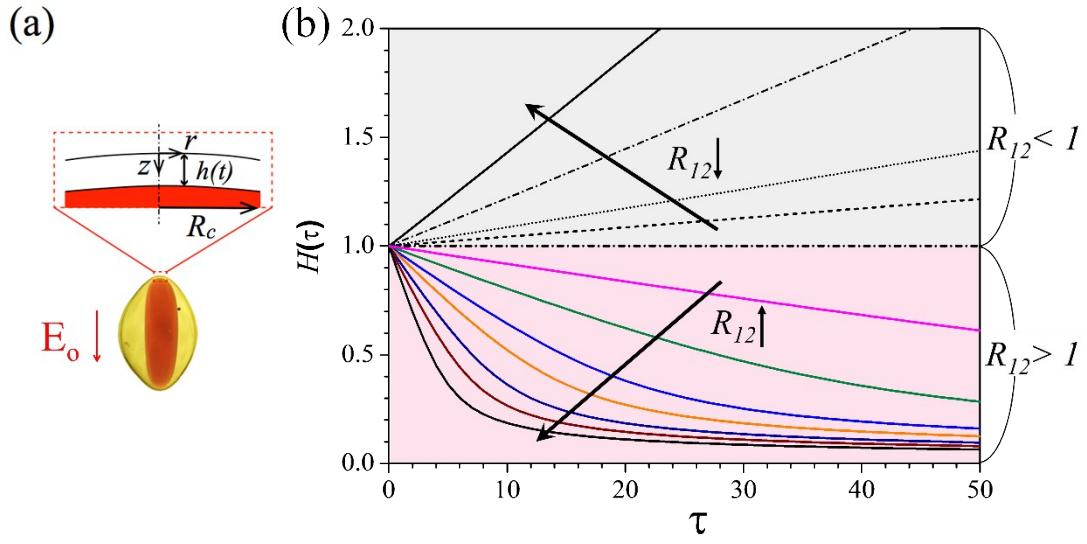

Fig. S10 (a) Schematic of the approaching core droplet toward the shell interface and the coordinates system. The thickness of the film of the shell liquid $h(t)$ is constant over $0 < r < R_c$ where R_c is the radius of the flat core surface under the DC electric field. (b) Nondimensionalized shell liquid thickness $H(\tau)$ plotted versus dimensionless shell liquid drainage timescale τ at different R_{12} conditions where $H = h(t)/h(0)$ and $\tau = t\left(\varepsilon_3 {E_0}^2 {h_0}^2\right)/\left(\mu_2 r^2\right)$. While the thin film increases in time at $R_{12} < 1$, the thin film gets thinner at $R_{12} > 1$ as time evolves. Here, $S_{12} = 1/S_{23}$, $R_{23} = 0.029$, E_o =2.95 kV/cm , $\beta = 0.5$ and $\mu_2 = 0.97$ Pa · s.

The flow is governed by the continuity equation and the incompressible Navier-Stokes equations under a uniform DC electric field,

$$\nabla \cdot \vec{u} = 0, \quad \rho\frac{D\vec{u}}{Dt} = -\nabla p + \mu_2 \nabla^2 \vec{u} + \nabla \cdot \sigma_M, \tag{S17a-b}$$

where $\vec{u} = (u_r, u_\theta, w)$ and μ_2 is the viscosity of the shell liquid. Here, the electric Maxwell stress jumps along the radial direction [see the coordinate system in Fig. S9 and Fig. S10 (a)] are negligible, i.e., $(\sigma_M \cdot \vec{n}) \cdot \vec{t} \simeq 0$ since $-\partial\phi/\partial r \simeq 0$ for the flat film surface. Moreover, since there is no bulk charge ($h_{crit} \gg \lambda_{EDL}$, where h_{crit} is the critical film thickness at rupture) or bulk permittivity change, the electric body force in the radial direction is negligible compared to the viscous and capillary pressure effects i.e. $\rho_e \vec{E} - \frac{1}{2}\varepsilon_o(\vec{E} \cdot \vec{E})\nabla\varepsilon \approx 0$. The Maxwell stress jump mainly acts along the *z*-direction. Due to the relatively thin film geometry, we use the lubrication equations in the cylindrical coordinate,

$$\frac{1}{r}\frac{\partial}{\partial r}(r u_r) + \frac{\partial u_z}{\partial z} = 0, \tag{S18a}$$

$$\frac{\partial p}{\partial r} \simeq \mu_2 \frac{\partial^2 u_r}{\partial z^2} \tag{S18b}$$

$$\frac{\partial p}{\partial z} \simeq \frac{\partial}{\partial z}\left((\sigma_M \cdot \vec{n}) \cdot \vec{n}\right) + \frac{\partial}{\partial z}\left((\sigma_H \cdot \vec{n}) \cdot \vec{n}\right) + \gamma\kappa, \tag{S18c}$$

where σ_M and σ_H are the Maxwell and hydrodynamic stresses, respectively, while κ is the curvature. In this case, we assume nearly flat surfaces (with zero curvature) at the onset, so $\kappa \approx 0$.[14]

The boundary conditions are

$$u_r(r,0) = 0, \tag{S19a}$$

$$u_r(r,h(t)) = 0, \tag{S19b}$$

$$u_z(r,h(t)) = \frac{dh}{dt}. \tag{S19c}$$

Using these boundary conditions, we obtain the velocity profile in the thin film, $u_r(r,z,t) = \left(1/2\mu_2\right)(\partial p/\partial r)z(z-h)$. Integrating this velocity profile with respect to z gives $\partial p/\partial r = \left(6\mu_2 r/h^3\right)(dh/dt)$. The pressure gradient occurs due to the Maxwell and hydrodynamic stress jumps;

therefore, at the side apex, the mean pressure distribution could be obtained from equation (S19c), $p(0,t) \simeq 81\varepsilon_3 {E_o}^2 \Psi^2 \{S_{23}(S_{12} - R_{12}^2)\}/2 - (2\chi\mu_2/\Gamma_{23} r)(dh/dt)$, where $\Psi = 1/[(R_{12}+2)(R_{23}+2) + 2\beta^3(R_{12}-1)(R_{23}-1)]$, while χ is the dimensionless number for the drag effect (see Equation S16) and the ambient pressure $p(\bar{\infty}, t)$ is relatively zero. In this case, we only consider the side apex and therefore the Maxwell stresses are almost uniform in each case. After the integration of the above equations with respect to *r,* the pressure distribution along the radial direction is

$$\bar{p(t)} = \frac{3\mu_2 r^2}{h^3} \frac{dh}{dt}, \qquad \text{(S20)}$$

where $0 < r < R_c$ and R_c is the radius of the flat core surface.

Equation (S20) can be non-dimensionalized with $R = r/R_c$, $H = h/h(0)$, $P = p/p(\bar{0}, t)$, and $\tau = t(\varepsilon_3 {E_0}^2 {h_0}^2)/(\mu_2 r^2)$, where τ is the shell fluid drainage time scale for the lubrication model, the initial film thickness $h_0 \equiv r_s - r_c$ and $R_c \equiv r_c$. Then, the resulting equation is

$$\frac{3}{H^3}\frac{dH}{d\tau} + \frac{2\chi {h_o}^3}{\Gamma_{23} {R_c}^3}\frac{dH}{d\tau} = \frac{81}{2}\Psi^2 S_{23}(S_{12} - {R_{12}}^2), \qquad \text{(S21)}$$

which describes the shell liquid film thinning at the side apex depending on the conductivity ratio and permittivity ratio between the core and shell. The initial condition at $\tau = 0$ is applied as $H(0) = 1$. Fig. S10(b) presents the time evolutions of the film thickness at $r = 0$, which is numerically obtained from equation (S21) by varying R_{12} while $R_{23} = 0.029$ and $S_{12}(= 1/S_{23}) = 1$. If the core is more conductive than the shell liquid, i.e. $R_{12} > 1$, the film thickness keeps decreasing with time. As long as R_{12} increases, the film gets thinner, rapidly. On the other hand, if $R_{12} < 1$, i.e., the core is less conductive than the shell liquid, the film gets thicker and eventually diverges after some finite time. These results are consistent with our experimental results (see Fig. S4 and Fig. S5 of ESI† and Supplementary movie 5). Furthermore, we observe that the analytical model successfully predicts the experimental results as shown in Fig. S11 in which the gap h(0) and h(t) are directly measured from experiments.

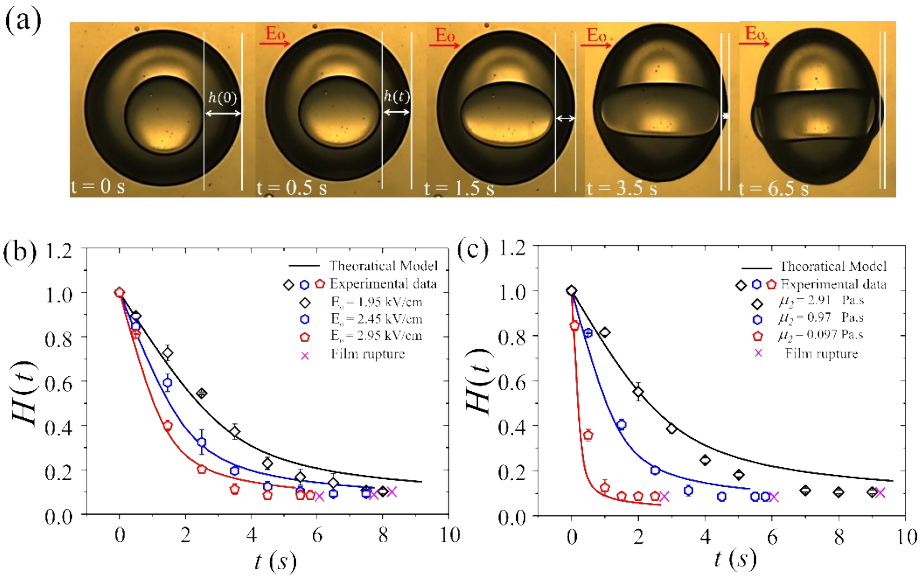

Fig. S11 Evolution of the core droplet in the double emulsion droplet. (a) Experimental results for the core elongation under the electric field. The gap thickness $h(t)$ is directly measured between the core side apex and shell interface where the experimental conditions are $E_0 = 2.45kV/cm, \beta \sim 0.5$ and $R_{12}/S_{12} = 23.45$. (b-c) Comparison between experimental and theoretical model (equation (S21)) results for the film drainage in double emulsion droplet under direct current electric field leading to bidirectional breakup (Mode II). (b) At different electric field strength (E_0) with μ_2 = 0.97 Pa · s. (c) At different viscosity of shell liquid (μ_2) with E_0 = 2.95 kV/cm. The condition of the experiment and theoretical model is $\beta \sim 0.5$ and $R_{12}/S_{12} = 23.45$. The filled cross symbols correspond to the film rupture stage as observed in the experiments.

VIII. Unstable bimodal breakup

We observe some unstable bimodal breakup, that the core first migrates towards the side apex and after coming in contact with the shell, the trailing end of the core disintegrates. We speculate that the electric Maxwell stresses on the core are non-uniform in this case where the trailing end of the core experiences large stresses that are responsible for this disintegration. We observe that this mode is transient that could occur between unidirectional and bidirectional breakup modes, having features that are resonant of both modes. Depending on the strength of the Maxwell stresses that scales with the applied electric field, we also observed the core streaming (the core trailing end forms sharp tips and ejects tiny droplets) and the core breaking with capillary instability (the core forms a thread that disintegrates into tiny droplets) for very small cores ($\beta < 0.3$) under high electric capillary number ($Ca_{23} > 1$), as shown in **Fig. S12.**

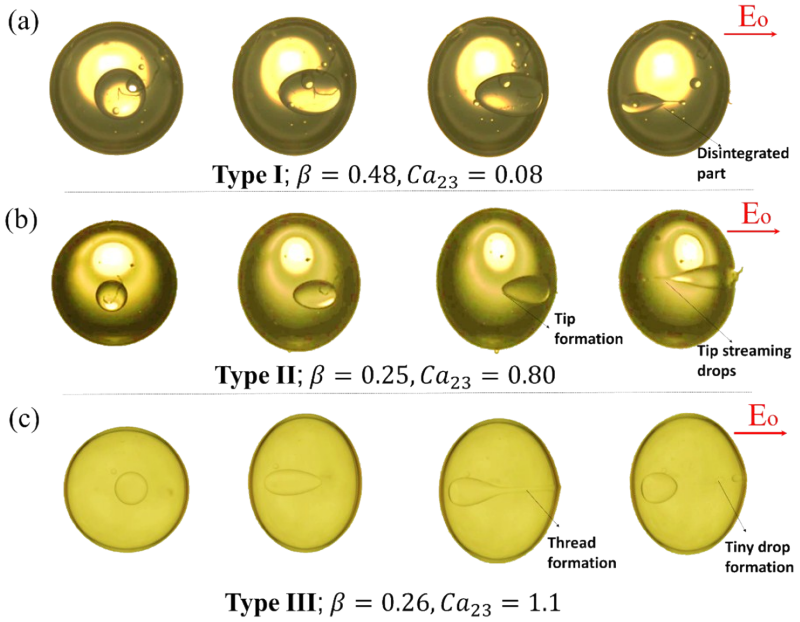

Fig. S12 Unstable bimodal breakup. Similar core disintegration cases are observed in the experiments at different conditions. (a) Type I: Fraction of core disintegrates during breakup. (b) Type II: Core tip streaming. The core forms cone at one end which streams tiny droplets. (c) Type III: Core breaks with capillary instability. The core makes thread that disintegrate in to satellite drops. We note that the ambient liquid in all the cases is pure castor oil. For all cases, $\Gamma_{23} = 1/\Gamma_{12} = 3.73$ and $R_{12}/S_{12} = 23.45$.

References

1. G. Taylor, *Proceedings of the Royal Society of London. Series A. Mathematical and Physical Sciences*, 1966, **291**, 159-166.
2. P. Dommersnes, Z. Rozynek, A. Mikkelsen, R. Castberg, K. Kjerstad, K. Hersvik and J. Otto Fossum, *Nature Communications*, 2013, **4**, 2066.
3. M. Ouriemi and P. M. Vlahovska, *Langmuir*, 2015, **31**, 6298-6305.
4. S. Torza, R. Cox and S. Mason, *Philosophical Transactions of the Royal Society of London A: Mathematical, Physical and Engineering Sciences*, 1971, **269**, 295-319.
5. M. Z. Bazant, *Journal of Fluid Mechanics*, 2015, **782**, 1-4.
6. O. Schnitzer and E. Yariv, *Journal of Fluid Mechanics*, 2015, **773**, 1-33.
7. D. Choi, H. Lee, D. J. Im, I. S. Kang, G. Lim, D. S. Kim and K. H. Kang, *Scientific Reports*, 2013, **3**, 2037.
8. J. H. Masliyah and S. Bhattacharjee, *Electrokinetic and colloid transport phenomena*, John Wiley & Sons, 2006.
9. D. A. Saville, *Annual Review of Fluid Mechanics*, 1997, **29**, 27-64.
10. K. Ahmad, C. Ho, W. Fong and D. Toji, *Journal of Colloid and Interface Science*, 1996, **181**, 595-604.
11. A. Estrada-Fernández, A. Román-Guerrero, R. Jiménez-Alvarado, C. Lobato-Calleros, J. Alvarez-Ramirez and E. Vernon-Carter, *Journal of Food Engineering*, 2018, **221**, 35-44.
12. C. Wang, M. Li, Y. Song, X. Pan and D. Li, *Electrophoresis*, 2018, **39**, 807-815.
13. A. Behjatian and A. Esmaeeli, *Physical Review E*, 2013, **88**, 033012.
14. D. Y. Chan, E. Klaseboer and R. Manica, *Soft Matter*, 2011, **7**, 2235-2264.